2007

Atmospheric Scaling of Cosmogenic Nuclide Production: Climate Effect

Jane Staiger

John Gosse

Rick Toracinta

Bob Oglesby

James Fastook

See next page for additional authors

Atmospheric scaling of cosmogenic nuclide production: Climate effect

Jane Staiger,[1,2] John Gosse,[1] Rick Toracinta,[3,4] Bob Oglesby,[5,6] James Fastook,[7] and Jesse V. Johnson[8]

Received 2 May 2005; revised 12 August 2006; accepted 18 September 2006; published 24 February 2007.

[1] Absorption of cosmic rays by atmospheric mass varies temporally due to a redistribution of atmospheric pressure by ice sheets during glaciations, the compression and expansion of the atmosphere due to cooling and warming, and changes in katabatic winds near large ice masses. These atmospheric processes can result in changes in production rates of cosmogenic nuclides which, when integrated over long exposure durations may result in 0% to >5% adjustments in site production rates depending on location. Combining a CCM3 model with imbedded ice sheets for 20 ka, we show that production rates changes (relative to today) are greatest at high elevations (6–7% at 5 km altitude) due to atmospheric compression from decreased temperature. Production rates at specific times for sites near ice sheet margins can be reduced more than 10% due to a combination of katabatic winds draining off the ice sheet margins and atmospheric cooling. Nunatak settings may be significantly affected by the climate effect due to persistent glacial atmospheric conditions. Atmospheric variability may explain some of the disparities among cosmogenic nuclide production rate calibrations.

Citation: Staiger, J., J. Gosse, R. Toracinta, B. Oglesby, J. Fastook, and J. V. Johnson (2007), Atmospheric scaling of cosmogenic nuclide production: Climate effect, *J. Geophys. Res.*, *112*, B02205, doi:10.1029/2005JB003811.

1. Introduction

[2] The production rate of terrestrial in situ cosmogenic nuclides (TCN) varies spatially and temporally with geomagnetic field strength and atmospheric pressure [*Lal*, 1991]. Production rates for six TCN (^{3}He, ^{10}Be, ^{14}C, ^{21}Ne, ^{28}Al, ^{36}Cl) have been determined for middle- and high-latitude sites at a range of atmospheric depths (from near sea level to >3000 m a.s.l.) and the technique has been used on surfaces spanning the elevations below sea level to >5000 m. Analytical measurements currently have routine precisions approaching 1% (1σ) but the uncertainty in time-averaged TCN production rates at some sites may be as large as 20% [*Gosse and Phillips*, 2001].

[3] Production rates measured at calibration sites are normalized to production at sea level and high latitude using algorithms derived mostly from detections of nuclear disintegrations (stars) in photographic film at different latitudes and altitudes [*Lal and Peters*, 1967; *Lal*, 1991] and/or from neutron flux measurements at different latitudes and altitudes (shipboard and monitor data) [e.g., *Dunai*, 2000; *Desilets and Zreda*, 2001, 2003]. All empirical calibrations are a time-integrated measurement over the independently determined (typically with radiocarbon or ^{40}Ar/^{39}Ar) exposure duration. Therefore each calibration incorporates the time varying geomagnetic [*Pigati and Lifton*, 2004] and atmospheric effects [*Stone*, 2000] specific to that site. The normalized production rates are averaged and then scaled, using the same algorithms, to calculate the TCN production rate at any site on Earth's surface. Improved scaling methods incorporating better fits of the nondipole geomagnetic field and nonstandard atmospheric pressure anomalies have been suggested by *Dunai* [2000] and *Stone* [2000], respectively. Uncertainties in the latitudinal scaling due to geomagnetic influences (especially due to temporal variations in paleointensity, secular variations in dipole position, and nondipole features of the geomagnetic field) have been addressed by others [*Gosse and Phillips*, 2001; *Masarik et al.*, 2001; *Dunai*, 2001; *Desilets and Zreda*, 2003; *Pigati and Lifton*, 2004] although there is no agreement on the actual influence of temporal variations in these geomagnetic field aspects. Uncertainty in atmospheric scaling has been assessed even less. *Stone* [2000] provided scaling factors for latitude and altitude based on those of *Lal* [1991] but recast the simple standard atmosphere approximation in terms of spatially variant atmospheric pressure. Even after rescaling the ^{10}Be production rates in quartz for a smaller muonic contribution (relative to *Lal* [1991]) there

[1]Department of Earth Sciences, Dalhousie University, Halifax, Nova Scotia, Canada.
[2]Now at the National Center for Earth-Surface Dynamics, St. Anthony Falls Laboratory, University of Minnesota-Twin Cities, Minneapolis, Minnesota, USA.
[3]Byrd Polar Research Center, Ohio State University, Columbus, Ohio, USA.
[4]Deceased 22 November 2005.
[5]NASA Marshall Space Flight Center, Huntsville, Alabama, USA.
[6]Now at Department of Geosciences, University of Nebraska at Lincoln, Lincoln, Nebraska, USA.
[7]Department of Computer Science, University of Maine, Orono, Maine, USA.
[8]Department of Computer Science, University of Montana, Missoula, Montana, USA.

0148-0227/07/2005JB003811$09.00

remains a slight positive correlation with calibration site elevation [*Gosse and Stone*, 2001].

[4] This work examines the influences on TCN production rates of changes in the atmospheric density distribution during glaciations. The principal objective of this paper is to consider the potential sources of atmospheric-derived influences on TCN production rates and we have attempted to quantify the effects. Interglacial and glacial conditions, discussed here as the difference between present day and the Last Glacial Maximum (LGM) climate, affects the total atmospheric mass that shields surface samples from cosmic radiation. Four conditions that arise from a change in climate are (1) changes in global atmospheric dynamics because ice sheets displace atmospheric mass, (2) quasi-stationary zones of low surface pressure at ice sheet margins [*Stone*, 2000] due to katabatic winds, (3) atmospheric compression due to cooling [*Dunai*, 2000], and (4) decreased degassing due to colder ocean temperatures decreases the global atmospheric mass [*Mélières et al.*, 1991]. Changes in the total mass of the atmosphere (condition 4) are calculated to be approximately 0.1% of the total atmospheric pressure [*Mélières et al.*, 1991] so will not be treated further due to the insignificant impact on TCN production rates. We evaluate the potential influence of the first three conditions and show that climate change may explain residual disparities among production rate calibrations for ^{10}Be and ^{3}He.

2. Methodology

[5] We used a General Circulation Model (GCM) to provide climate simulations at two different climate scenarios, present day conditions and LGM conditions, to determine the effect of large ice sheets on the atmosphere [*Toracinta et al.*, 2004]. Note that climate change without growth or decay of glaciers can have an impact on production rates, but the presence of ice sheets significantly adds to this effect and enables us to evaluate the affect of climate at two end-member climate regimes. The LGM GCM incorporated global glacier ice cover as calculated by the thermomechanical University of Maine Ice Sheet Model (2003 version) (UMISM [*Fastook and Chapman*, 1989; *Fastook and Prentice*, 1994]). Full methodology for simulated LGM ice sheet surface elevations and simulated LGM atmospheric conditions from a GCM that includes a Land Surface Model (LSM) are described elsewhere (CCM3 [*Kiehl et al.*, 1998a, 1998b] and LSM (*Bonan* [1998] as cited by *Toracinta et al.* [2004])). The following sections give an overview of the boundary conditions and nature of these models.

2.1. UMISM

[6] UMISM is a time-dependant, momentum and mass-balance driven, finite-element model. Temperature proxy data from the GRIP ice core drives the ice sheet response and is extrapolated outward radially and with lapse rates that govern temperature with altitude [*Fastook and Chapman*, 1989; *Fastook and Prentice*, 1994]. Recent improvements in UMISM include additions of glacio-isostacy, thermodynamics of the temperature distribution within the ice sheet, and basal water algorithms [*Johnson and Fastook*, 2002]. These improvements allow better control on ice-margin position and ice sheet surface elevation and are crucial to developing reasonable estimates of the effect of LGM climate on TCN production rates, especially at (calibration) sites that lie on the margins of paleo-ice sheets.

[7] The surface elevations include an isostatic adjustment such that a pseudo-elastic, hydrostatically supported crust is depressed by the weight of glacier ice. However, areas beyond the ice sheet margins are not isostatically compensated. These temporary ice proximal depressions near ice margins are typically on the order of up to tens of meters and would not likely affect the climate simulations or TCN production rates. The climate in UMISM was controlled by the δ^{18}O curve from the GRIP ice core, central Greenland transformed to a temperature record [*Johnsen et al.*, 1995]. This record therefore forms the backbone of the temperature and precipitation calculation that drives the glacial cycle. The mean annual temperature for each node varies by specified altitudinal and latitudinal lapse rates.

[8] For the LGM climate simulations, Laurentide, Fennoscandian, and Antarctic ice sheet elevations are the glaciological model output from UMISM. The Patagonian Ice Sheet elevations are from model output by *Hulton et al.* [2002]. Sea level during the LGM was lowered by 120 m, commensurate with the LGM ice sheet volume. Calculated sea level provides an additional check on global ice volume calculations.

[9] The major uncertainty in UMISM is the input mass balance, which must be simulated for a full glacial cycle. However, the ice sheet configuration is only slightly sensitive to errors in the mass balance. An analytic treatment of a flat-bedded, uniform-accumulation elliptical profile shows that thickness is proportional to accumulation rate raised to the 1/8th power. Hence an error of a factor of 2 in the accumulation rate only produces a 10% error in the thickness.

2.2. CCM3

[10] The NCAR Community Climate Model version 3 (CCM3 [*Kiehl et al.*, 1998a]) is used to simulate the LGM climate over the ice sheets prescribed by UMISM. Boundary conditions other than UMISM ice elevations include 21-kyr computed orbital parameters for solar forcing, trace gases concentration (CO_2 concentration set to 180 ppm; CH_4 concentration set to 350 ppbv), sea level, and a modified version of the CLIMAP SSTs based on proxy data (a different temperature modeling scheme than UMISM). Modern vegetation was used due to uncertainty in global vegetation reconstructions for the LGM. The model employs a T42 spectral truncation (2.8° × 2.8° transform grid) with 18 levels in the vertical [*Toracinta et al.*, 2004].

[11] Present day topographic input is based on a 64 × 128-cell grid (2.8° × 2.8°) that coarsely samples topography. The performance of CCM3 in simulating the present day climate is described in several papers in the *Journal of Climate* special issue (June 1998). CCM3 produces a reasonable representation of the large-scale atmospheric circulation including the Northern Hemisphere longwave pattern and zonal wind structure [*Kiehl et al.*, 1998a]. Large-scale surface pressure features are well captured, as are the midlatitude storm tracks [*Hurrell et al.*, 1998; *Kageyama et al.*, 1998]. Tropical interseasonal oscillations

are simulated by CCM3, albeit with shorter than observed periodicities and somewhat damped amplitudes.

[12] The simulated top-of-atmosphere radiative budget agrees well with observations, although deficiencies in the treatment of clouds in marine stratus regions and in the placement of atmospheric deep convection in the western Pacific result in large biases in shortwave fluxes at the surface and top-of-atmosphere [*Kiehl et al.*, 1998b]. The hydrologic cycle is generally well simulated, as is the Indian Monsoon, although CCM3 produces a lower tropospheric dry bias in the large-scale moisture field [*Hack et al.*, 1998].

[13] In polar regions, CCM3 exhibits deficiencies in the simulated radiation budget that are related to an excessive cloud fraction and cloud water path [*Briegleb and Bromwich*, 1998a]. The resulting negative biases in solar radiation budget result in deep polar vortices and cold surface temperatures compared to observations [*Briegleb and Bromwich*, 1998b]. Also, errors in surface albedo result from the lack of a meltwater pond representation in CCM3 and other atmospheric changes that may be specific to LGM conditions like the effect of large proglacial or pluvial lakes [*Hostetler et al.*, 2000]. While CCM3 generally captures many important polar atmospheric features, there are errors in amplitude and placement of, for instance, the Northern Hemisphere Icelandic Low and Aleutian Low as well as the Antarctic circumpolar trough [*Briegleb and Bromwich*, 1998b]. The Antarctic katabatic wind regime is well captured. A strong similarity between the CCM3 atmospheric simulation for present day and the compilation of 50-year averaged atmospheric data shown by *Stone* [2000] further demonstrates the reliability of the GCM model output.

[14] The LGM surface elevation input is based on the model output of UMISM and present day elevations outside the margins of the ice sheets. Eustatic LGM sea level lowering is treated by raising the topography by 120 m and classifying subaerial regions between 0 and 120 m below sea level as new land surface. The atmospheric changes solely due to the displacement of sea level are not trivial and are addressed by *Osmaston* [2006] and are implicit in the CCM3 simulation. The simulation conforms to general knowledge of LGM climate and matches specific LGM proxy data (alkenone, borehole, coral Sr/Ca ratio, emu eggshell, faunal/foraminifera, noble gases, ice core stable isotope, Mg/Ca ratio, pollen, and radiolaria) [*Toracinta et al.*, 2004]. At the latitudes of most production rate calibration sites (>40°), the average CCM3 simulation temperature anomalies (LGM minus present; 8.9°C) match average proxy record temperature anomalies (9.1°C) the best [*Toracinta et al.*, 2004]. The calculations of changes in surface pressure due to changes in atmospheric temperature are the least uncertain of the CCM3 functions and the cause of the greatest surface pressure changes. The interannual variability in surface pressure lies in the range of 1–2 hPa for the majority of the atmosphere over landmass, but in active storm zones (i.e., Icelandic Low), the variability can be as great as 4–6 hPa.

2.3. Production Rate Calculations

[15] Sea level of the LGM model run is 120 m below present-day sea level. For the comparison of LGM and present day surface pressures, adjustments to modeled pressure are unnecessary since surface pressure refers to the total mass above the surface. The calculations presented here build on the original altitude and latitude scaling method of *Lal* [1991], which assumed an atmosphere with a uniform pressure of 1013.5 hPa. *Stone* [2000] adjusted *Lal*'s [1991] altitude and latitude scaling equations in terms of atmospheric pressure (P, in hPa) rather than altitude. *Stone*'s [2000] scaling factor for production by spallation used in this calculation is

$$S(P) = a + b\exp[-P/150] + cP + dP^2 + eP^3. \quad (1)$$

Coefficients "a," "b," "c," "d," and "e" are given for latitudes of 0°–60° in 10° increments [*Stone*, 2000, Table 1]. Values between the 10° increments are linearly interpolated.

[16] The contribution of muons is considered negligible in this calculation in order to keep the results applicable to all TCN. This treatment of muons is warranted because muons contribute only a few percent of the total surface production of TCN at sea level and decreases with decreasing atmospheric pressure or elevation [*Stone*, 2000; *Kubik and Ivy-Ochs*, 2004].

3. Results

[17] GCM output shows significant differences between the LGM 200 hPa height field and the present-day 200 hPa height field (Figure 1). Compression of the atmosphere has an observably nonsymmetric change on global air pressure. Areas that are most affected by changes in pressure due to climate change are illustrated in the graphs of latitudinally averaged deviations of pressures (Figure 2). These areas that are most affected are located near the margins of paleo-ice sheets or are located at latitudes with high average elevations. At the high-altitude sites, atmospheric compression during glaciation essentially results in a migration of atmospheric mass to lower elevations (Figure 3), such that at sea level, the effect of atmosphere compression is negligible, but at 3.5 km above sea level, the TCN production rate can be 3–4% greater than the present day atmosphere.

[18] A rough estimate of the validity of the CCM3 atmospheric compression is supported by equilibrium line altitude (ELA) changes during the LGM in the tropics. *Porter*'s [2001] review of snowline depression in the tropics cited 900 ± 135 m of lowering during the LGM owing to decreased atmospheric temperatures. Using environmental lapse rates (ELR) range of 6.5°C/km or 10°C/km, this change in the ELA corresponds to 10.4 to 4.9°C of cooling in this area. Assuming that the ELA corresponds to the 0°C isotherm for tropical glaciers and using the universal gas law (PV = nRT) [*Osmaston*, 2006], this results in 1.8% to 3.8% decrease in the volume of the atmosphere. The CCM3 simulation of LGM atmospheric compression produces a 300 m decrease of the height of the 200-hPa isobar in this area, which is 3% of the average height of the 200-hPa isobar. This CCM3 simulation value lies within the range of compression supported by changes in the snowline altitudes [*Porter*, 2001].

[19] The deviation of LGM production rates from present day due to changes in atmosphere conditions is shown in Figure 4. This result therefore incorporates the effect observed by *Stone* [2000] regarding the error in assuming

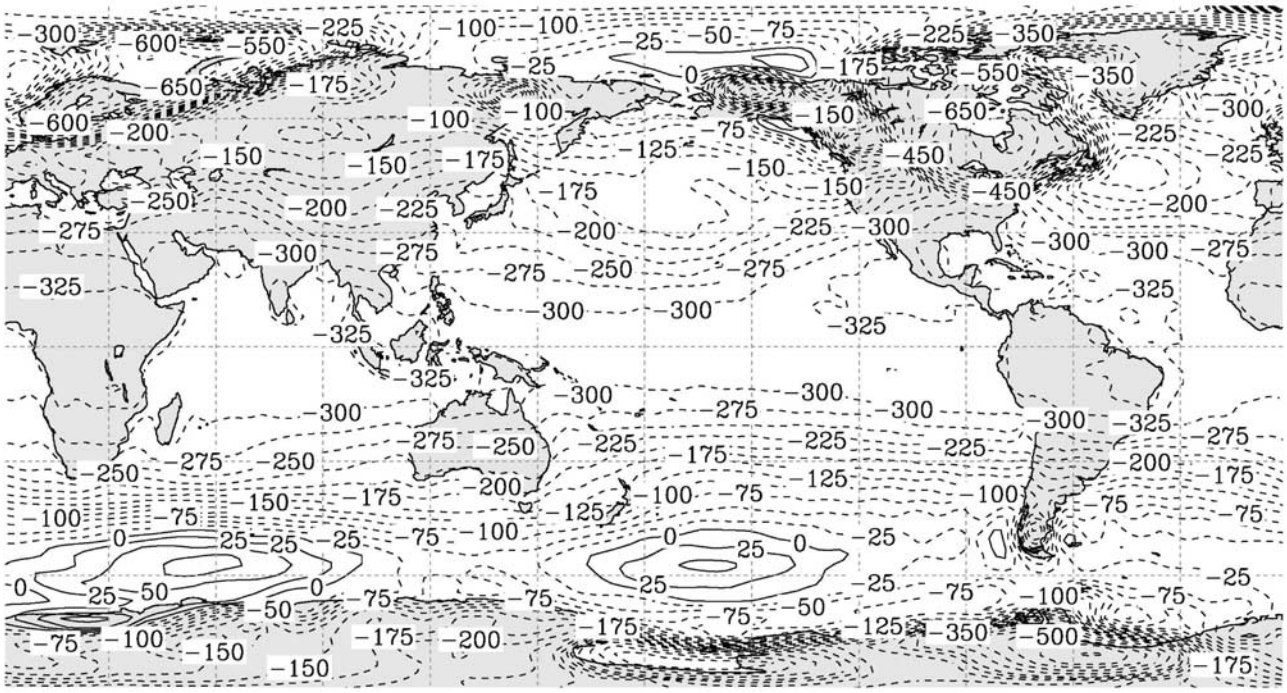

Figure 1. Difference in 200 mb height field between 15-year average LGM and 15-year average (modeled) present-day CCM3-simulation output. Dashed contours (m) reflect a compressed atmosphere; the deviation is greatest in areas near paleo-ice sheets. Solid contours signify a locally expanded atmosphere due to effects of glaciation.

a globally uniform standard atmosphere as well as the effect of the significant variations in atmospheric pressure distribution with time. On average, the difference in the LGM and present day simulation surface pressure is approximately 8 hPa, which, as stated above, is greater than the interannual variability of the CCM3 model (1–2 hPa) in most places and even greater than rare locally high interannual variability of 4–6 hPa. For most areas, the uncertainty in the production rate changes due to the effect of changing climate during the LGM is less than ±25%.

4. Discussion

[20] The deviations shown in Figure 4 are maximum differences between the two end-member glacial and nonglacial modeled scenarios. Because TCN concentrations increase with exposure duration, a TCN exposure age reflects an integration of the time-varying production rates. To adjust the production rates over a glacial cycle, one must interpolate between the glacial production rate and the interglacial production rate by a fitting function that is appropriate to the glacial setting. For example, the production rate interpolation from an LGM (+6.5% correction) to present-day (0% correction after *Stone* [2000] is applied) of a boulder on a terminal moraine of an ice sheet at 5.7 km altitude which was occupied by an oscillating ice margin for 5 ka before rapid retreat would have to be adjusted for all three conditions (katabatic winds associated with the ice sheet for the first 5 ka of exposure, and the atmospheric variations due to cooling and the presence of ice sheets for the entire exposure duration, Figure 5). On the other hand, a surface at sea level far removed from an ice sheet would experience a negligible integrated effect over the past 21 ka. The largest katabatic wind effect during a single glaciation would occur in areas where there has been a long-standing ice margin or on nunataks. On the basis of the distribution of erratic exposure ages from the front to rear of the broad

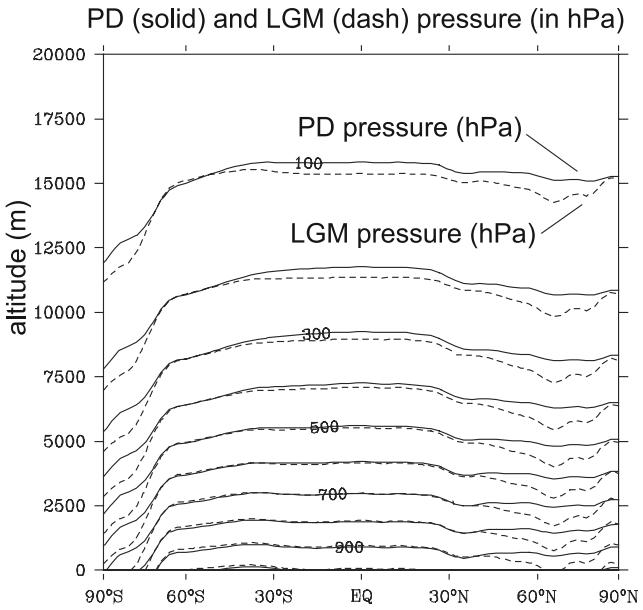

Figure 2. Longitudinal cross-section of average simulated pressure are contoured from 1000 to 100 (hPa) for present-day (solid lines) and LGM (dashed). Altitude represents height above the contemporaneous sea level.

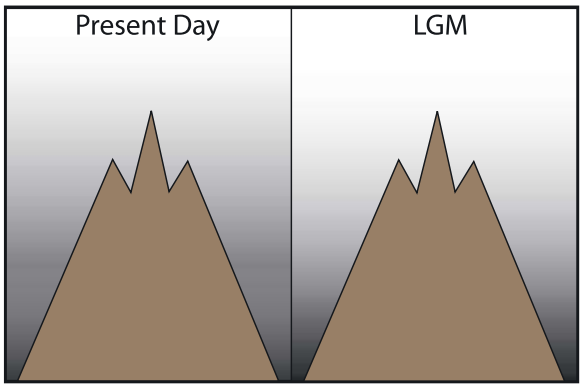

Figure 3. Illustration of atmosphere density redistribution due to cooling. The darkness of the shading of the background corresponds to atmospheric pressure (mass). Total mass is equal for both times. TCN production rates will not vary at sea level, but at high elevation production rates will be greater during periods of glaciation.

moraine, *Gosse et al.* [1995] have showed that ice occupancy of the large LGM terminal moraine of the Fremont Lake lobe (Rocky Mountain Pinedale Glaciation type locality) may have persisted for more than 5 ka. Importantly, for exposure durations than span beyond the last 21 ka, the time integrated climate effect on production rates will be larger considering that ice sheets modified the atmosphere for the majority of the Pleistocene.

[21] The influence of the climate conditions on TCN production rates can be evaluated for any calibration site. For example, the influence of katabatic winds may be significant (>2%) when integrated over the entire exposure duration. *Ackert et al.* [2003] have cited anomalies in their long-term ^{3}He production rates from Patagonian lava flows, independently dated by ^{40}Ar/^{39}Ar that are 11% higher than other published ^{3}He production rates. They attributed the higher rate to atmospheric effects. Their long-term production rate is supported by our model results, which show ~8% greater (glacial) production than modeled present day production. When tuned to a δ^{18}O temperature record and integrated over the duration of exposure, the production rate change in this area is 4–5% for the flows of different ages. An additional 4% greater production can be explained by the error related to using a standard atmosphere instead of a more realistic atmosphere [*Stone*, 2000].

[22] After rescaling ^{10}Be production rates measured at calibration sites for a lower muonic contribution than *Lal* [1991], *Stone* [2000] noted a small, residual positive correlation between published ^{10}Be production rates and elevation [*Gosse and Stone*, 2001]. The combined effects of the atmospheric changes may explain why low elevation calibration sites [e.g., *Clark et al.*, 1996; *Stone et al.*, 1998] yield 4 to 6% lower production rates than the average of all sites. The higher elevation sites may be influenced more by atmospheric compression (which results in less shielding) and at least one of the low elevation sites is strongly influenced by katabatic winds (from the Laurentide Ice Sheet). Figure 6 illustrates the influence of climate related time-integrated adjustments in production rates at sites where ^{10}Be has been measured. In the case of the New Jersey Laurentide Ice Sheet (LIS) calibration site adjustment, we

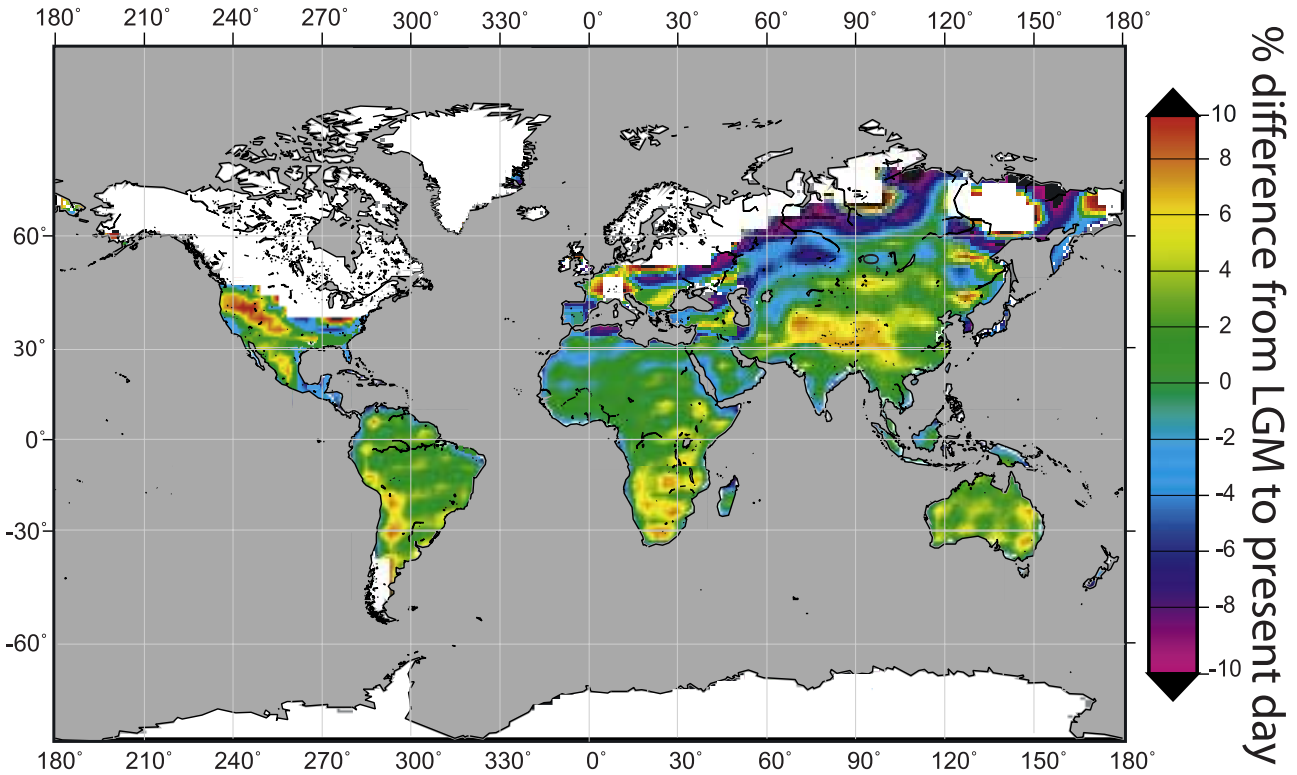

Figure 4. Percentage deviation of LGM production rates from present-day production rates. White areas were glaciated during the LGM and are excluded from the calculation.

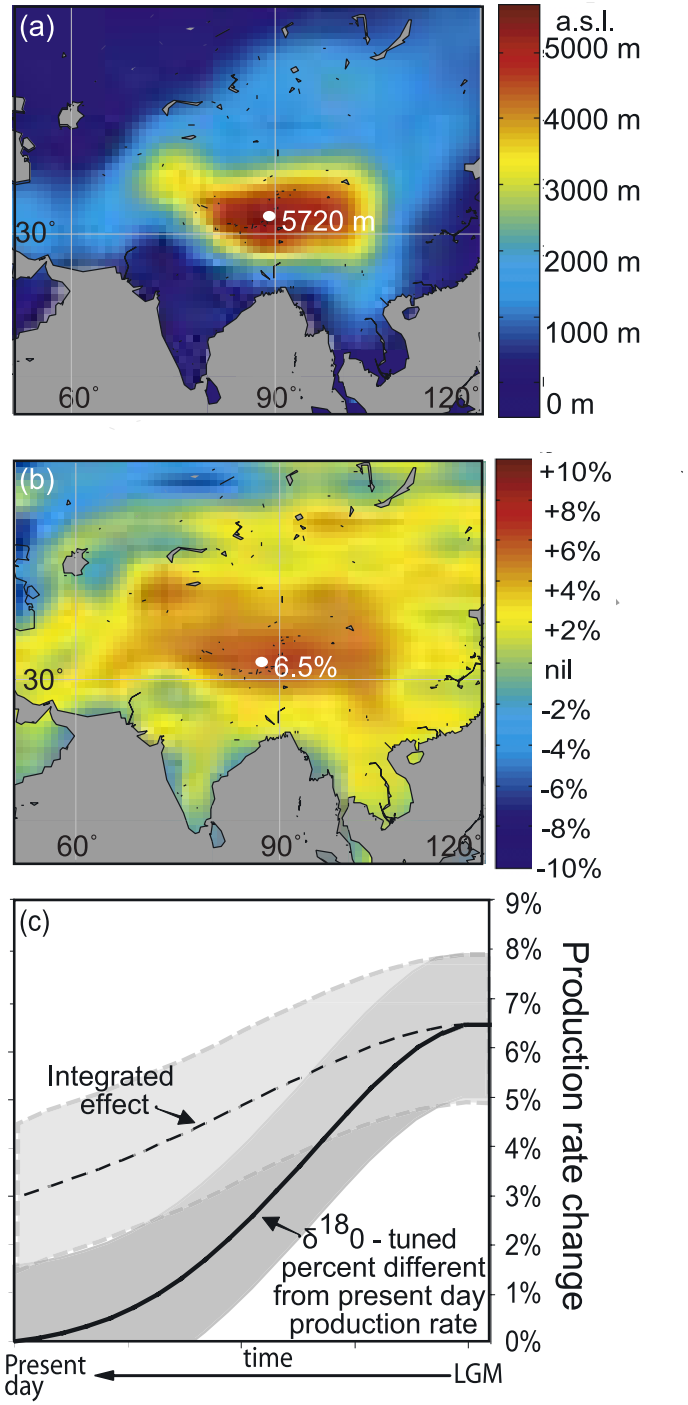

Figure 5. (a) Surface elevations (present day) of the Himalaya used in the model climate simulations. (b) Production rate percentage difference between present day and LGM conditions. The area experiencing the greatest difference grossly matches the topography, illustrating the dominance of the atmospheric compression effect at high elevations. (c) The 5720 m elevation site in Figure 5a with a production rate increase of 6.5% during the LGM relative to present day may follow a $\delta^{18}O$ temperature curve to the present day correction of 0%. The noise in the model output (1–2 hPa) introduces an uncertainty of 1.5% in the change in the production rate and is shown by a gray band outlining the curve. The total effect on production rates in a sample deposited during the LGM follows the dashed line that essentially accumulates all the production rates to a final production rate adjustment of approximately 3% (±1.5%) over that time of exposure.

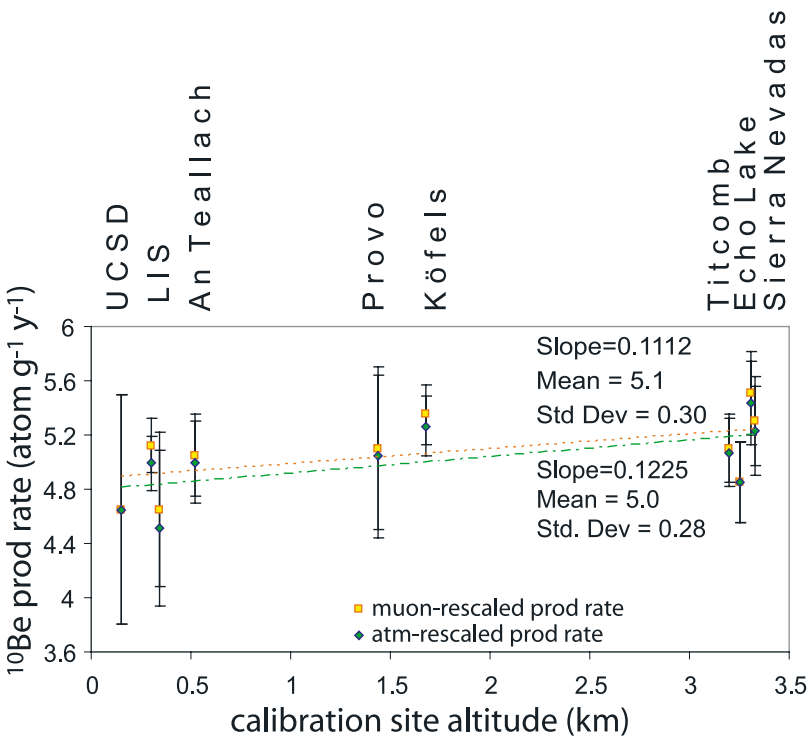

Figure 6. Calibrated and measured production rates of ^{10}Be (yellow squares) versus altitude, adapted from *Gosse and Stone* [2001]. LIS [*Larsen et al.*, 1995; *Bierman et al.*, 1996]; An Teallach [*Stone et al.*, 1998]; Provo [*Gosse et al.*, 1995]; Köfels [*Kubik and Ivy-Ochs*, 2004]; Titcomb Basin [*Gosse and Klein*, 1996]; and Sierra Nevada [*Nishiizumi et al.*, 1989; *Clark et al.*, 1996]. These production rates are scaled by *Lal*'s [1991] formulation to SLHL (sea level, high geomagnetic latitude) but uses a muonic contribution of 2.2% [*Stone*, 2000], except for the Köfels site which uses a 3% muonic contribution. The green diamonds mark the correction of the ^{10}Be production rates for LGM atmospheric deviations from present day that includes a δ^{18}O curve fit from LGM production rate deviation to present day, integrated over the period of exposure.

report the production rate adjusted by length of time the calibration site was in close proximity to the ice margin [*Larsen*, 1995, and references therein; *Larsen et al.*, 1995]. The production rates derived from UCSD and Echo Lake artificial targets [*Nishiizumi et al.*, 1996] have not been adjusted for the LGM climate effect. The production rate adjustments due to atmospheric effects decrease the average production rate by 2% and slightly improve the standard deviation of the production rates. However, these adjustments are within 1 standard deviation of the mean of the published calibrated ^{10}Be production rates, 5.1 ± 0.3 atom g^{-1} a^{-1} [*Gosse and Stone*, 2001]. At this time, the topographic resolution of the CCM3 climate model inhibits more precise adjustments for site specific calibrations.

5. Conclusions

[23] Three climate-controlled atmospheric conditions induce temporal variability in TCN production rates. Decreases in atmospheric pressure due to katabatic winds will increase production rates near the margins of large glaciers. The difference between present day and LGM production rates due to katabatic winds may be larger than 10% in places. Atmospheric compression due to cooling will result in higher TCN production rates with greater elevation relative to present day atmospheric conditions. Changes in the synoptic atmospheric pressure distribution due to cooling and the increased volume of ice masses lead to spatial variations in global atmospheric dynamics. The latter two conditions have caused glacial climate production rates to be as much as 7% higher than the present day in some areas. The magnitude of the time-integrated changes in production rates will be proportional to the amount of the total exposure duration that experienced glaciation or multiple glaciations. Although quantifications of the impact of climate induced atmospheric changes on TCN production rates were attempted, the uncertainty in the CCM3 and UMISM simulations is not fully quantified and therefore our results can only be considered estimates. The implication of climate-induced TCN production rate variability for published and future calibrations will require some consideration as the community continues to improve the TCN dating technique.

[24] **Acknowledgments.** We thank Djordje Grujic and Rasmus C. Thiede for the use of the Excel spreadsheet for calculating mean linear regressions and the late Henry Osmaston for stimulating discussions on the appropriate treatment of sea level lowering during the LGM. The Laurentide Ice Sheet research project was sponsored by NSF grant OPP-9905381. The project was funded by ACOA-AIF grant 1001052 to J.G. J.S. thanks the Killam Trust for funding through a Doctoral Fellowship Award. The final manuscript editing was supported by the NCED, a Science and Technology Center funded by the Office of Integrative Activities of the National Science Foundation (EAR-0120914).

References

Ackert, R. P., B. S. Singer, H. Guillou, M. R. Kaplan, and M. D. Kurz (2003), Long-term cosmogenic ^{3}He production rates from ^{40}Ar/^{39}Ar and K-Ar dated Patagonian lava flows at 47°S, *Earth Planet. Sci. Lett.*, *210*, 119–136.

Bierman, P. R., P. Larsen, E. Clapp, and D. Clark (1996), Refining estimates of ^{10}Be and ^{26}Al production rates, *Radiocarbon*, *38*, 149.

Bonan, G. B. (1998), The land surface climatology of the NCAR land surface model (LSM1.0) coupled to the NCAR Community Climate Model (CCM3), *J. Clim.*, *11*, 1307–1326.

Briegleb, B. P., and D. H. Bromwich (1998a), Polar radiation budgets of the NCAR CCM3, *J. Clim.*, *11*, 1246–1269.

Briegleb, B. P., and D. H. Bromwich (1998b), Polar climate simulation of the NCAR CCM3, *J. Clim.*, *11*, 1270–1286.

Clark, D. H., P. Bierman, and A. R. Gillespie (1996), ^{10}Be and ^{26}Al production rates and a revised glacial chronology for the Sierra Nevada, *Radiocarbon*, *38*, 152.

Desilets, D., and M. Zreda (2001), On scaling cosmogenic nuclide production rates for altitude and latitude using cosmic-ray measurements, *Earth Planet. Sci. Lett.*, *193*, 213–225.

Desilets, D., and M. Zreda (2003), Spatial and temporal distribution of secondary cosmic-ray nucleon intensities and applications to in situ cosmogenic dating, *Earth Planet. Sci. Lett.*, *206*, 21–42.

Dunai, T. J. (2000), Scaling factors for production rates of in situ produced cosmogenic nuclides: A critical reevaluation, *Earth Planet. Sci. Lett.*, *176*, 157–169.

Dunai, T. J. (2001), Influence of secular variation of the geomagnetic field on production rates of in situ produced cosmogenic nuclides, *Earth Planet. Sci. Lett.*, *193*, 197–212.

Fastook, J., and J. Chapman (1989), A map plane finite-element model: Three modeling experiments, *J. Glaciol.*, *35*, 48–52.

Fastook, J., and M. Prentice (1994), A finite-element model of Antarctica: Sensitivity test for meteorological mass balance relationship, *J. Glaciol.*, *40*, 167–175.

Gosse, J. C., and J. Klein (1996), Production rate of in situ cosmogenic (super 10) Be in quartz at high altitude and mid latitude, *Radiocarbon*, *38*, 154–155.

Gosse, J. C., and F. M. Phillips (2001), Terrestrial in situ cosmogenic nuclides: Theory and applications, *Quat. Sci. Rev.*, *40*, 1475–1560.

Gosse, J. C., and J. O. Stone (2001), Terrestrial cosmogenic nuclide methods passing milestones of paleo-altimetry, *Eos Trans. AGU*, *82*(7), 82, 86, 89.

Gosse, J. C., J. Klein, E. B. Evenson, B. Lawn, and R. Middleton (1995), Be-10 dating of the duration and retreat of the last Pinedale Glacial Sequence, *Science*, *268*, 1329–1333.

Hack, J. J., J. T. Kiehl, and J. W. Hurrell (1998), The hydrologic and thermodynamic characteristics of the NCAR CCM3, *J. Clim.*, *11*, 1179–1206.

Hostetler, S. W., P. J. Bartlein, P. U. Clark, E. E. Small, and A. M. Solomon (2000), Simulated influences of Lake Agassiz on the climate of central North America 11,000 years ago, *Nature*, *405*, 334–337.

Hulton, N. R., R. S. Purves, R. D. McColloch, D. E. Sugden, and M. J. Bentley (2002), The Last Glacial Maximum and deglaciation of southern South America, *Quat. Sci. Rev.*, *21*, 233–241.

Hurrell, J. W., J. J. Hack, B. A. Boville, D. L. Williamson, and J. T. Kiehl (1998), The dynamical simulation of the NCAR Community Climate Model Version 3 (CCM3), *J. Clim.*, *11*, 1207–1236.

Johnsen, S., D. Dahl-Jensen, W. Dansgaard, and N. Gunderup (1995), Greenland paleotemperatures derived from GRIP bole hole temperature and ice core isotope profiles, *Tellus, Ser. B*, *47*, 624–629.

Johnson, J. V., and J. L. Fastook (2002), Northern Hemisphere glaciation and its sensitivity to basal melt water, *Q. Int.*, *95–96*, 65–74.

Kageyama, M., P. J. Valdes, G. Ramstein, C. Hewitt, and U. Wyputta (1998), Northern Hemisphere storm tracks in present day and last glacial maximum climate simulations: A comparison of the European PMIP models, *J. Clim.*, *12*, 742–760.

Kiehl, J. T., J. J. Hack, G. B. Bonan, B. A. Boville, D. L. Williamson, and P. J. Rasch (1998a), The National Center for Atmospheric Research Community Climate Model: CCM3, *J. Clim.*, *11*, 1131–1149.

Kiehl, J. T., J. J. Hack, and J. W. Hurrell (1998b), The energy budget of the NCAR Community Climate Model: CCM3, *J. Clim.*, *11*, 1151–1178.

Kubik, P. W., and S. Ivy-Ochs (2004), A re-evaluation of the 0–10 ka ^{10}Be production rate for exposure dating obtained from the Köfels (Austria) landslide, *Nucl. Instrum. Methods Phys. Res., Sect. B*, *223–224*, 618–622.

Lal, D. (1991), Cosmic ray labeling or erosion surfaces: In situ nuclide production rates and erosion models, *Earth Planet. Sci. Lett.*, *104*, 424–439.

Lal, D., and B. Peters (1967), Cosmic-ray produced radioactivity on the earth, *Handb. Phys.*, *46*, 512–551.

Larsen, P. (1995), In situ production rates of cosmogenic ^{10}Be and ^{26}Al over the past 21,500 years determined from the terminal moraine of the Laurentide ice sheet, north central New Jersey, M. S. thesis, Univ. of Vt., Burlington.

Larsen, P. L., P. R. Bierman, and M. Caffee (1995), Preliminary in situ production rates of cosmogenic ^{10}Be and ^{26}Al over the past 21.5 ky from the terminal moraine of the Laurentide ice sheet, north-central New Jersey, *Geol. Soc. Am. Abstr. Prog.*, *27*, A59.

Masarik, J., M. Frank, J. M. Schäfer, and R. Wieler (2001), Correction of in situ cosmogenic nuclide production rates for geomagnetic field intensity variations during the past 800,000 years, *Geochim. Cosmochim. Acta*, *65*, 2995–3003.

Mélières, M. A., P. Martinerie, D. Rayraud, and L. Lliboutry (1991), Glacial-interglacial mean sea level pressure change due to sea level, ice sheet and atmospheric mass changes, *Palaeogeogr. Palaeoclimatol. Palaeoecol.*, *89*, 333–340.

Nishiizumi, K., C. P. Kohl, J. R. Arnold, E. L. Winterer, D. Lal, J. Klein, and R. Middleton (1989), Cosmic ray production rates of ^{10}Be and ^{26}Al in quartz from glacially polished rocks, *J. Geophys. Res.*, *94*, 17,907–17,915.

Nishiizumi, K., R. C. Finkel, J. Klein, and C. P. Kohl (1996), Cosmogenic production of ^{7}Be and ^{10}Be in water targets, *J. Geophys. Res.*, *101*, 22,225–22,232.

Osmaston, H. A. (2006), Should Quaternary sea-level changes be used to correct glacier ELAs, vegetation belt altitudes and sea level temperatures for inferring climate changes?, *Quat. Res.*, *65*, 244–251.

Pigati, J. S., and N. A. Lifton (2004), Geomagnetic effects on time-integrated cosmogenic nuclide production with emphasis on in situ ^{14}C and ^{10}Be, *Earth Planet. Sci. Lett.*, *226*, 193–205.

Porter, S. C. (2001), Snowline depression in the tropics during the last glaciation, *Quat. Sci. Rev.*, *20*, 1067–1091.

Stone, J. O. (2000), Air pressure and cosmogenic isotope production, *J. Geophys. Res.*, *105*, 23,753–23,759.

Stone, J. O., C. K. Ballantyne, and L. K. Fifield (1998), Exposure dating and validation of periglacial weathering limits, NW Scotland, *Geology*, *26*, 587–590.

Toracinta, E. R., R. J. Oglesby, and D. H. Bromwich (2004), Atmospheric response to modified CLIMAP ocean boundary conditions during the Last Glacial Maximum, *J. Clim.*, *17*, 504–522.

J. Fastook, Department of Computer Science, University of Maine, Orono, ME 04469, USA. (fastook@maine.edu)

J. Gosse, Department of Earth Sciences, Dalhousie University, 3006 Life Sciences Centre, Edsell Castle Circle, Halifax, NS, Canada B3H 4J. (john.gosse@dal.ca)

J. V. Johnson, Department of Computer Science, Social Science Building, Room 417, University of Montana, Missoula, MT 59812, USA. (johnson@cs.umt.edu)

B. Oglesby, Department of Geosciences, University of Nebraska at Lincoln, 214 Bessey Hall, Lincoln, NE 68588-0340, USA. (roglesby2@unl.edu)

J. Staiger, National Center for Earth-Surface Dynamics, St. Anthony Falls Laboratory, University of Minnesota-Twin Cities, 2 Third Avenue SE, Minneapolis, MN 55414, USA. (staig011@umn.edu)